

Supplementary Information

Efficient photocatalytic conversion of CH₄ into ethanol with O₂ over nitrogen vacancy-rich carbon nitride at room temperature

Zhongshan Yang,^{ab} Qiqi Zhang,^{ab} Liteng Ren,^{ab} Xin Chen,^{ab} Defa Wang,^{ab} Lequan Liu,^{*ab} and

Jinhua Ye^{abc}

^a TJU-NIMS International Collaboration Laboratory, Key Lab of Advanced Ceramics and Machining Technology (Ministry of Education) and Tianjin Key Laboratory of Composite and Functional Materials, School of Materials Science and Engineering, Tianjin University, 92 Weijin Road, Tianjin, P. R. China.

^b Collaborative Innovation Center of Chemical Science and Engineering (Tianjin), Tianjin 300072, P. R. China.

^c International Center for Materials Nanoarchitectonics (WPI-MANA), National Institute for Materials Science (NIMS) 1-1 Namiki, Tsukuba, Ibaraki 3050044, Japan.

Table of contents

Experimental sections.....	3
Figure S1. The SEM (A) and TEM (B) images of the CN sample.	6
Figure S2. The XRD patterns of CN and RCN sample.	7
Figure S3. The FT-IR spectra of CN & RCN-x samples.	8
Figure S4. The N 1s XPS spectra of CN and RCN-5.	9
Figure S5. Device diagram of photocatalytic conversion of methane experiments.	10
Figure S6. The spectrum of the incident light source and UV-vis spectrum of RCN-5.	11
Figure S7. The GC spectrum of CO ₂ produced over CN in photocatalytic conversion of methane.	12
Figure S8. ¹ H NMR of methane oxidation product over RCN-5.	13
Figure S9. Photocatalytic methane conversion over different amount of RCN-5.	14
Figure S10. Control experimental results of the photocatalytic reaction over RCN-5.	15
Figure S11. Average production rate of methane conversion over CN and RCN-5 samples in 10 h without illumination.	16
Figure S12. XRD patterns of RCN-5 before and after reaction.	17
Figure S13. TEM image of RCN-5 after reaction.	18
Figure S14. PL spectra of 1 mM coumarin solution over CN and RCN-5.	19
Figure S15. Photocatalytic H ₂ O ₂ production over RCN-5 with different reaction time.	20
Figure S16. PL spectra of CN and RCN-5.	21
Figure S17. Electrochemical impedance spectroscopy for CN and RCN-5.	22
Table S1. Comparison of photocatalytic conversion of methane into ethanol over various catalyst reported at room temperature.	23
Table S2. C/N atomic ratio of CN and RCN samples from EA results.	24
Table S3. C/N atomic ratio of CN and RCN samples from XPS analysis.	25
Table S4. The multi-exponential fitting results of fluorescence decay for CN and RCN-5.	26
Reference.....	27

Experimental sections

Chemicals

All chemical reagents were purchased from *J&K Chemical* and *Aladdin*. All the chemical reagents were of analytical grade and used without any further purification.

Preparation of Samples

The synthesis of CN (g-C₃N₄) and RCN-*x* (reduced g-C₃N₄) was based on the investigation reported by Yanrong Zhang.^[1] Typically, 10 g melamine was placed into a crucible with a lid and then heated up to 450 °C for 4 h at a rate of 5 °C/min in a muffle furnace. The obtained product was grounded with an agate mortar and then washed with hot deionized water (80 °C) three times, also dried in vacuum at 70 °C for 12 h. The obtained whitish powder was denoted as CN. The RCN-*x* were thoroughly blended CN with different amount of NaBH₄ (*x* = 3, 5, 7, represents the weight ratio of CN:NaBH₄ were 1:3, 1:5, 1:7) in a mortar, and then thermally treated at 370 °C in argon atmosphere for 30 min with a heating rate of 5 °C/min. The product was washed with hot deionized water (80 °C) three times. Then it was dried in vacuum at 70 °C for 12 h. The obtained yellow powder was denoted as RCN-*x*.

Characterizations

The phase and crystal structure of the samples were performed on a powder X-ray diffraction (XRD, D/MAX 2500, Rigaku Co., Japan) with Cu K α radiation ($\lambda = 0.154$ nm). The morphology study was performed on a field emission scanning electron microscopy (FE-SEM, S4800, Hitachi, Japan) and a transmission electron microscopy (TEM, JEM-F200, JEOL, Japan). Fourier transform infrared spectroscopy (FT-IR) were recorded on a spectrometer (Nicolet-6700, Thermo Scientific, USA). N/C atomic ratio of CN and RCN was determined by an Elemental analyzer (Vario Micro cube, Elementar,

Germany). The electron spin resonance (ESR) spectra measurements were executed on JES-FA200 X-band spectrometer. The surface chemical analysis was investigated by X-ray photoelectron spectroscopy (XPS, ESCALAB-250Xi, Thermo Scientific, USA). The absorption spectra of the samples were converted from the UV-vis diffuse reflectance spectra measured on UV-vis spectrophotometer (UV-2700, Shimadzu, Japan). The photoluminescence (PL) spectrum measurements and fluorescence lifetimes were detected by a spectrofluorometer (Fluorolog-3, Horiba Jobin Yvon, USA) with an excitation wavelength of 375 nm.

Photocatalytic Activity Evaluation

Photocatalytic methane conversion experiments were carried out in a stainless-steel autoclave (Figure S1) containing a Teflon liner vessel (working volume, 50 mL) equipped with a quartz window to allow light irradiation. Typically, 20 mg catalyst was dispersed in 20 mL deionized water followed by ultrasonication for 5 min. The Teflon vessel was placed in the well of the autoclave, and the autoclave was sealed. Then, the sealed autoclave was pressurized with 0.1 MPa O₂ (purity, 99.999%) and 2 MPa CH₄ (purity, 99.999%) following purging O₂ five times. Subsequently, the autoclave was loaded into a water circulation system keeping the reaction temperature at 25±1 °C, and the solution was stirring at 200 rpm. 300 W Xe lamp (Figure S2, light intensity, 100 mW cm⁻²) was employed as the light source. Other experiments operated at different reaction conditions will be mentioned extra. The obtained liquid products were quantified by ¹H nuclear magnetic resonance (NMR, Avance III, Bruker, Germany, 400 MHz). Typically, 0.5 mL liquid product was mixed with 0.1 mL of D₂O, and 0.02 μL dimethyl sulfoxide (DMSO, Heowns, 99.9%) was added into as an internal standard. The gas phase

product was gleaned by a gas sampling bag and quantified by gas chromatography (GC, Shimadzu 2010) with a flame ionization detector (FID).

The concentration of H₂O₂ was quantified with a colorimetric DPD method. [2] The concentration of H₂O₂ was monitored by the absorption of the solution at 551 nm which was recorded using the UV-vis spectrometer.

Electrochemical measurements

The electrochemical measurements were carried out on an electrochemical workstation (CHI 760 E, Shanghai, China) with a three-electrode cell in an aqueous solution containing 0.1 M Na₂SO₄. The CN and RCN electrodes which were used as working electrodes were prepared by drop-coating on the FTO glass. The Ag/AgCl (3 M KCl) electrode and a Pt wire were employed as the reference electrode and counter electrode, respectively. All the potentials were referenced to the Ag/AgCl electrode without specification. The 300 W Xe lamp was used as the light source.

The ethanol selectivity was calculated through the following equation:

$$Selectivity = \frac{Productivity\ of\ ethanol}{Productivity\ of\ EtOH + Productivity\ of\ MeOH + Productivity\ of\ HCOOH + Productivity\ of\ CO_2} \quad (S1)$$

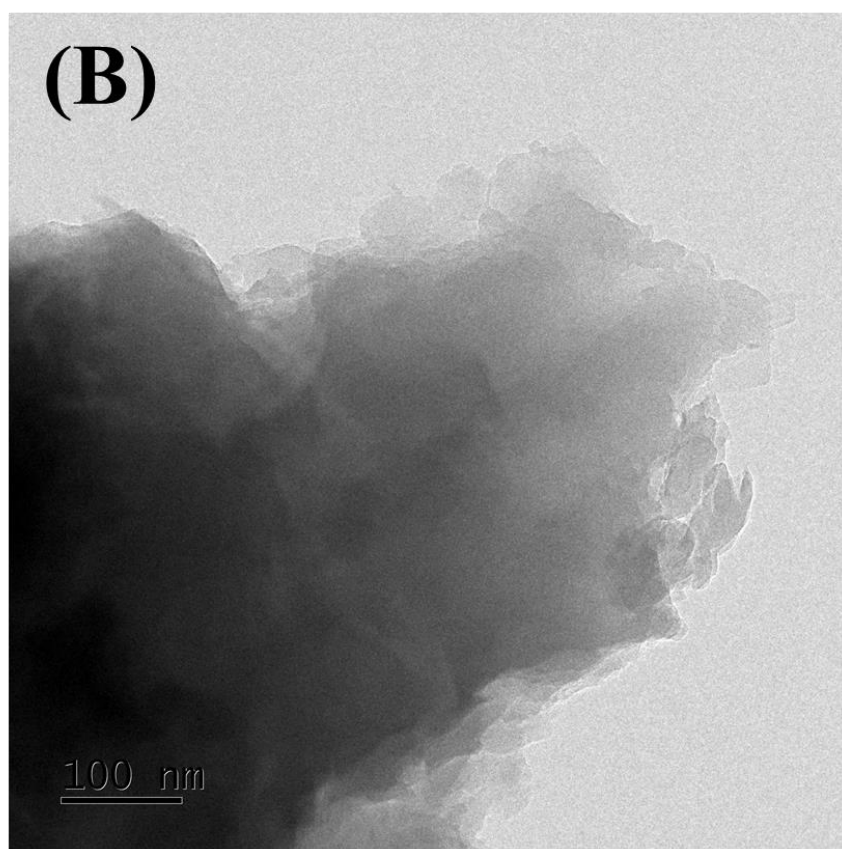
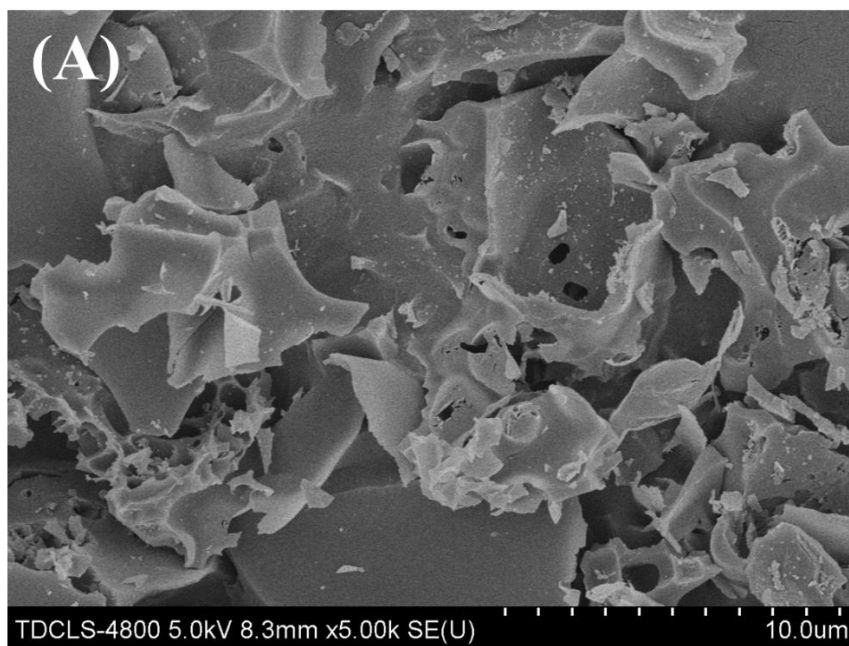


Figure S1. The SEM (A) and TEM (B) images of the CN sample.

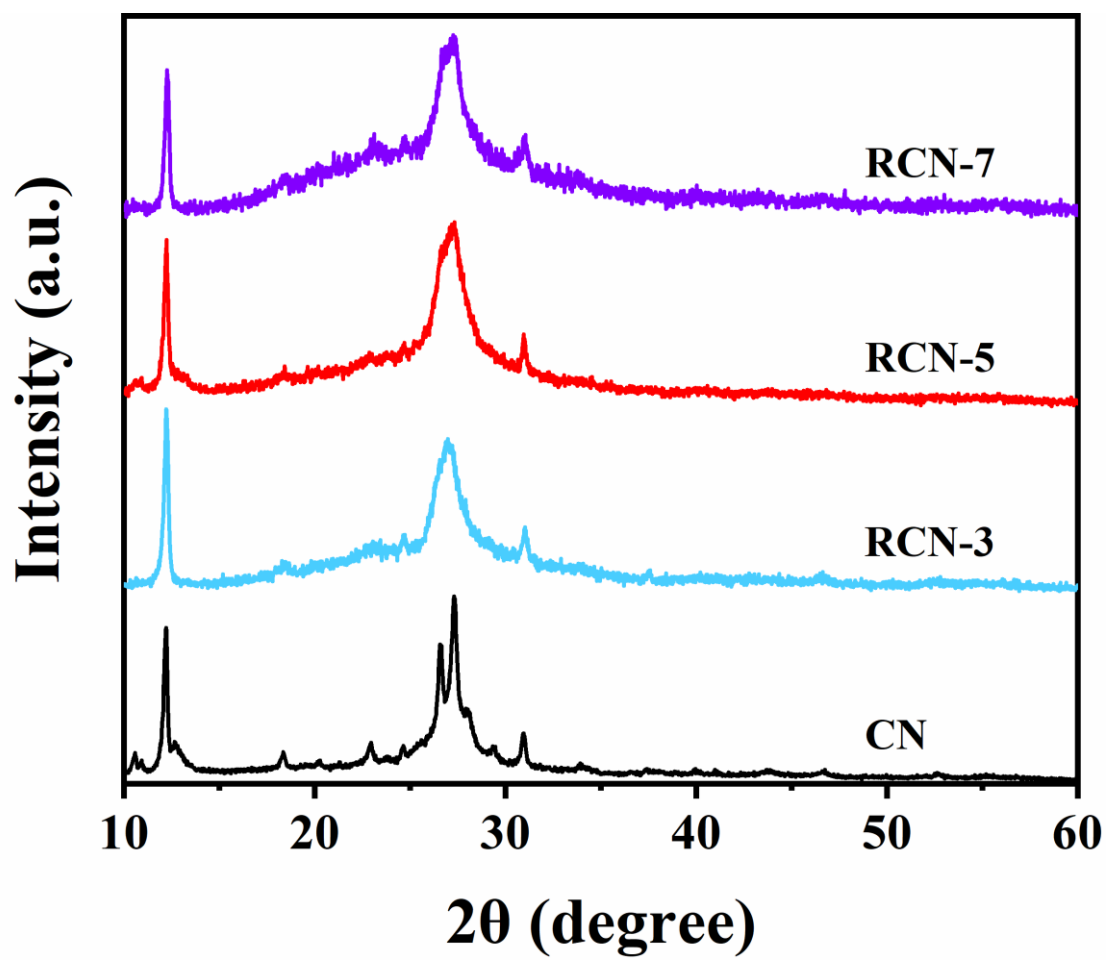


Figure S2. The XRD patterns of CN and RCN sample.

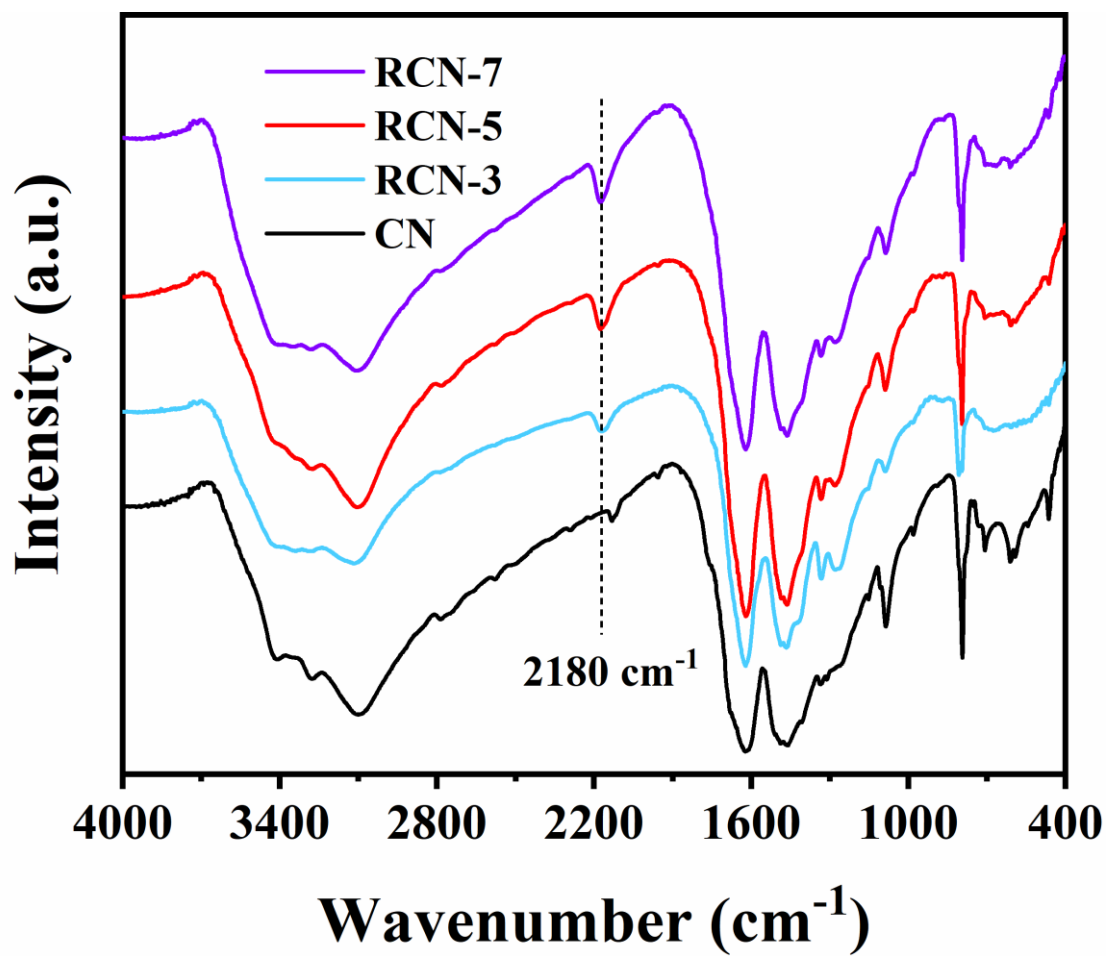


Figure S3. The FT-IR spectra of CN & RCN-x samples.

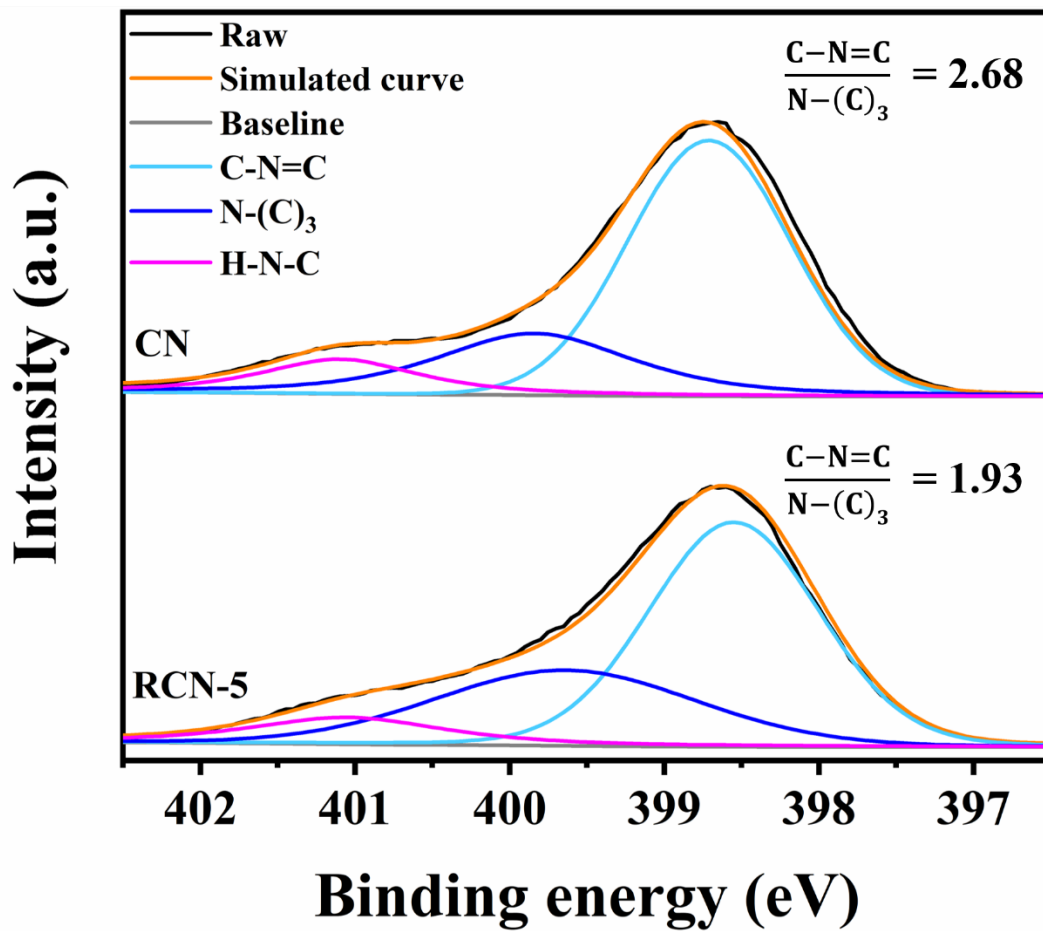


Figure S4. The N 1s XPS spectra of CN and RCN-5.

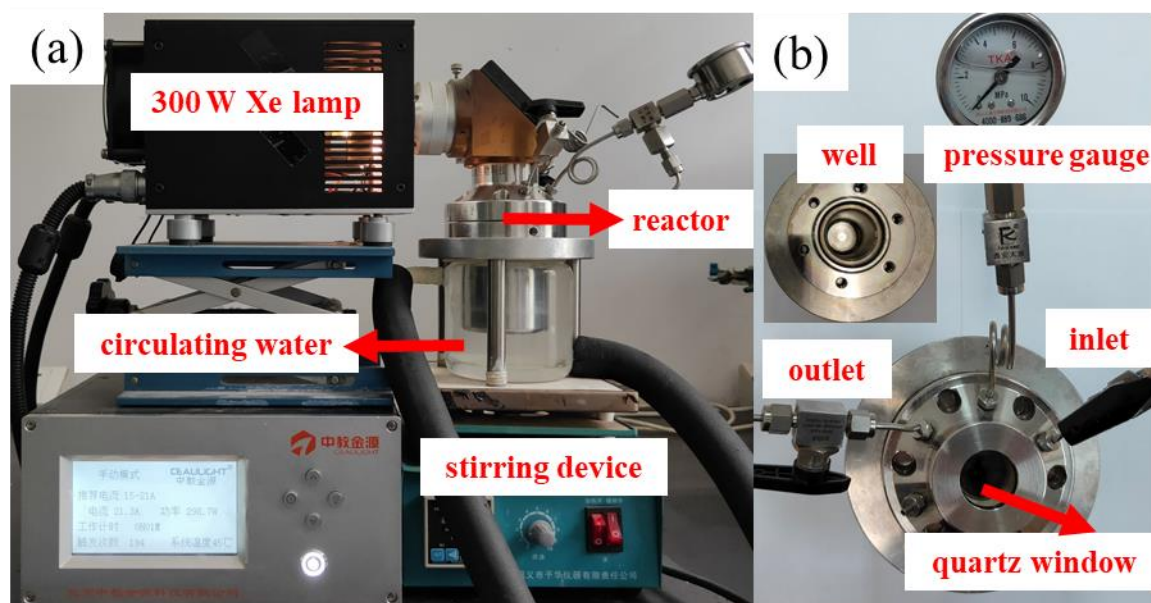


Figure S5. Device diagram of photocatalytic conversion of methane experiments.

- (a) The simple indication of light source, reactor, circulating water system and stirring device;
- (b) detailed structure of the used reactor.

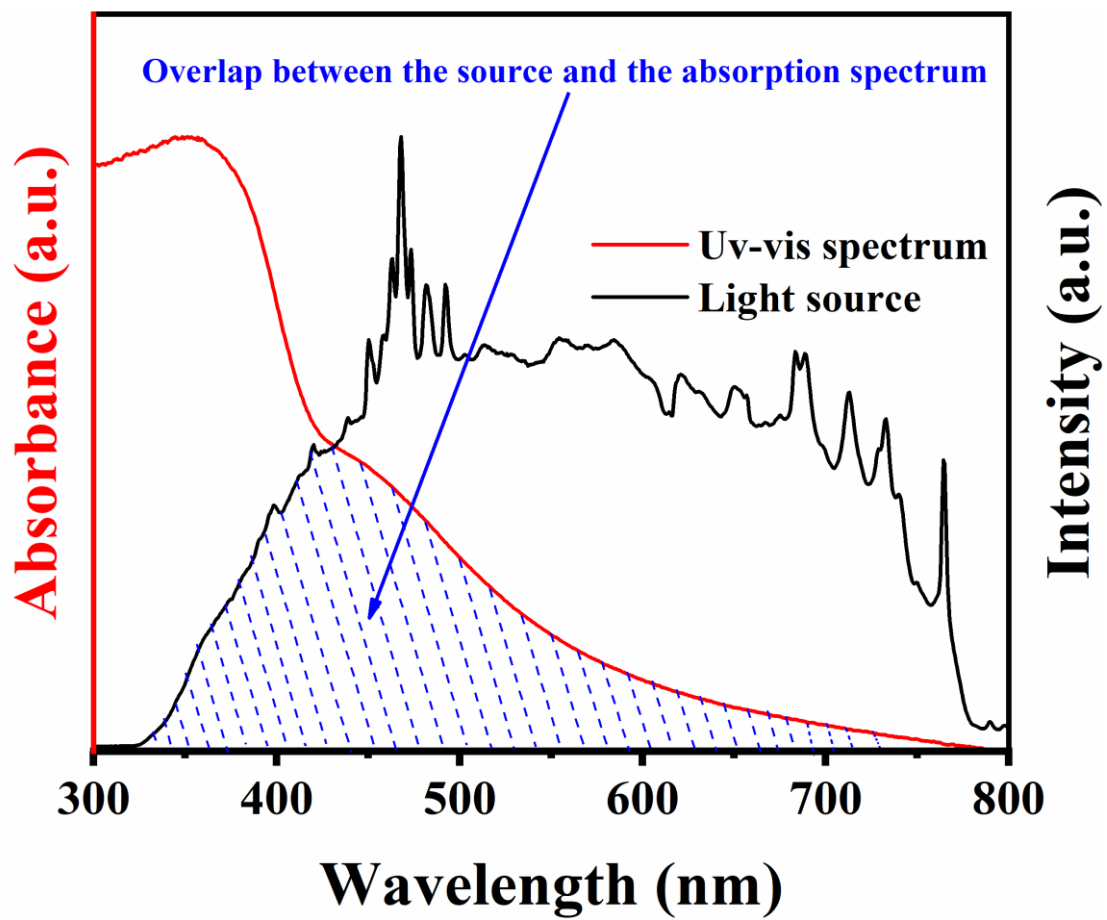


Figure S6. The spectrum of the incident light source and UV-vis spectrum of RCN-5.

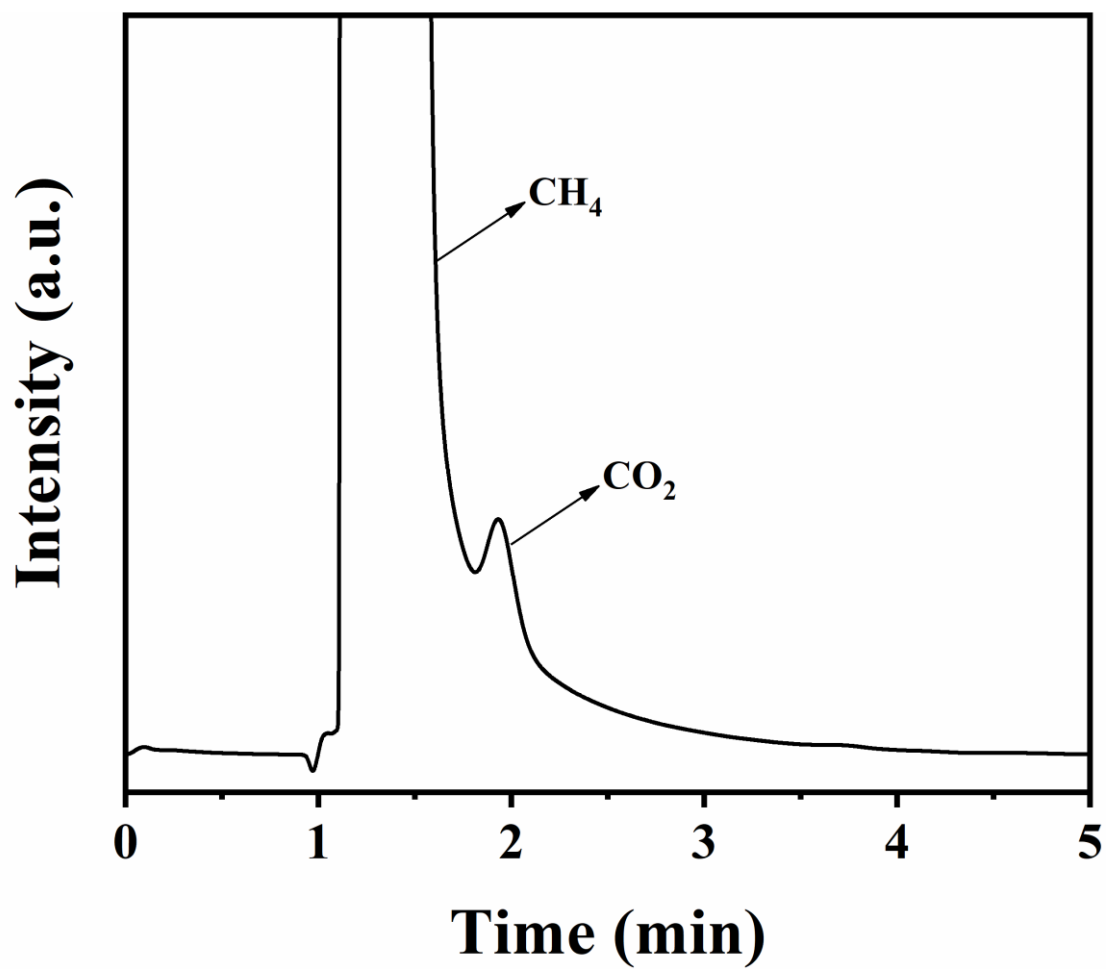


Figure S7. The GC spectrum of CO₂ produced over CN in photocatalytic conversion of methane.

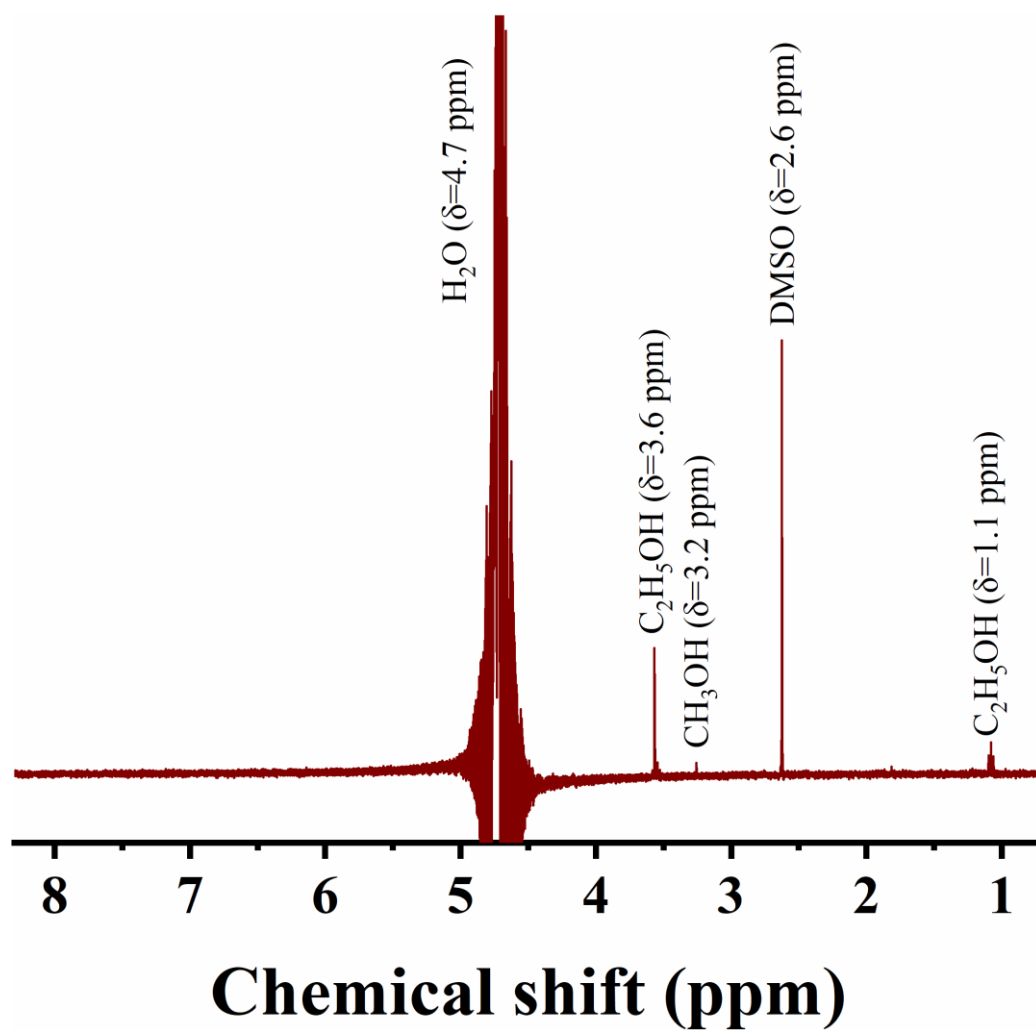


Figure S8. ^1H NMR of methane oxidation product over RCN-5.

DMSO was adopted as an internal standard in NMR test.

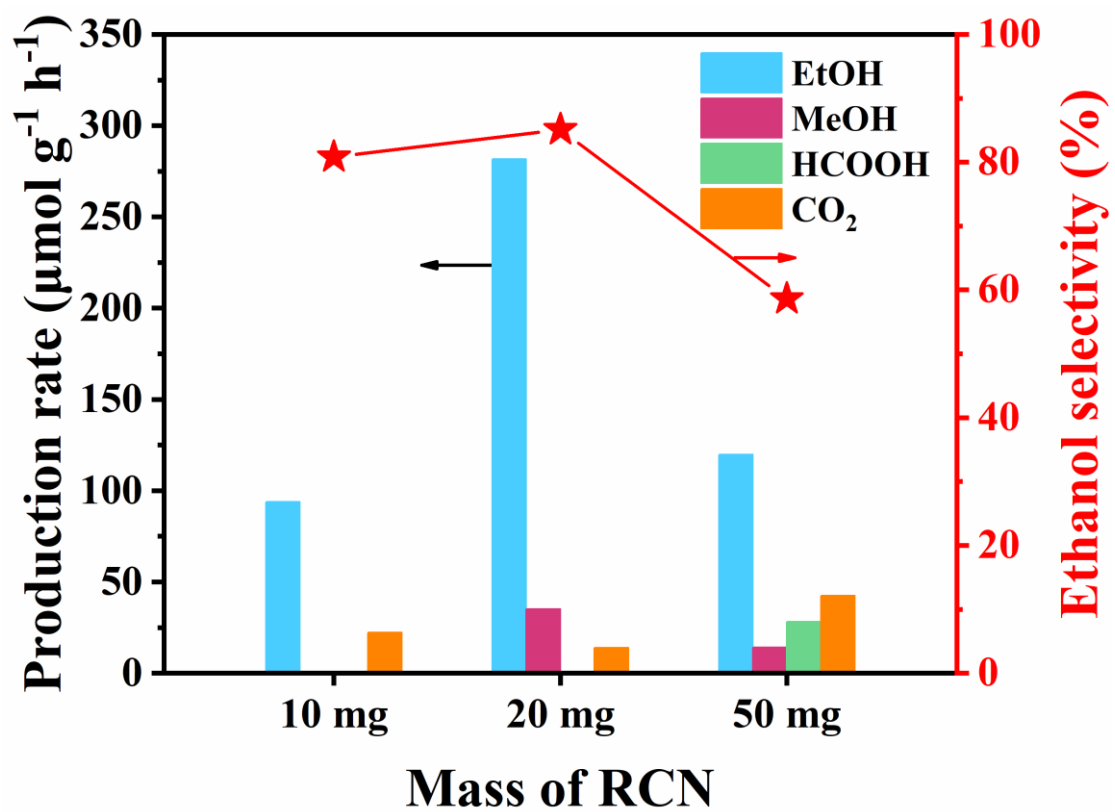


Figure S9. Photocatalytic methane conversion over different amount of RCN-5.

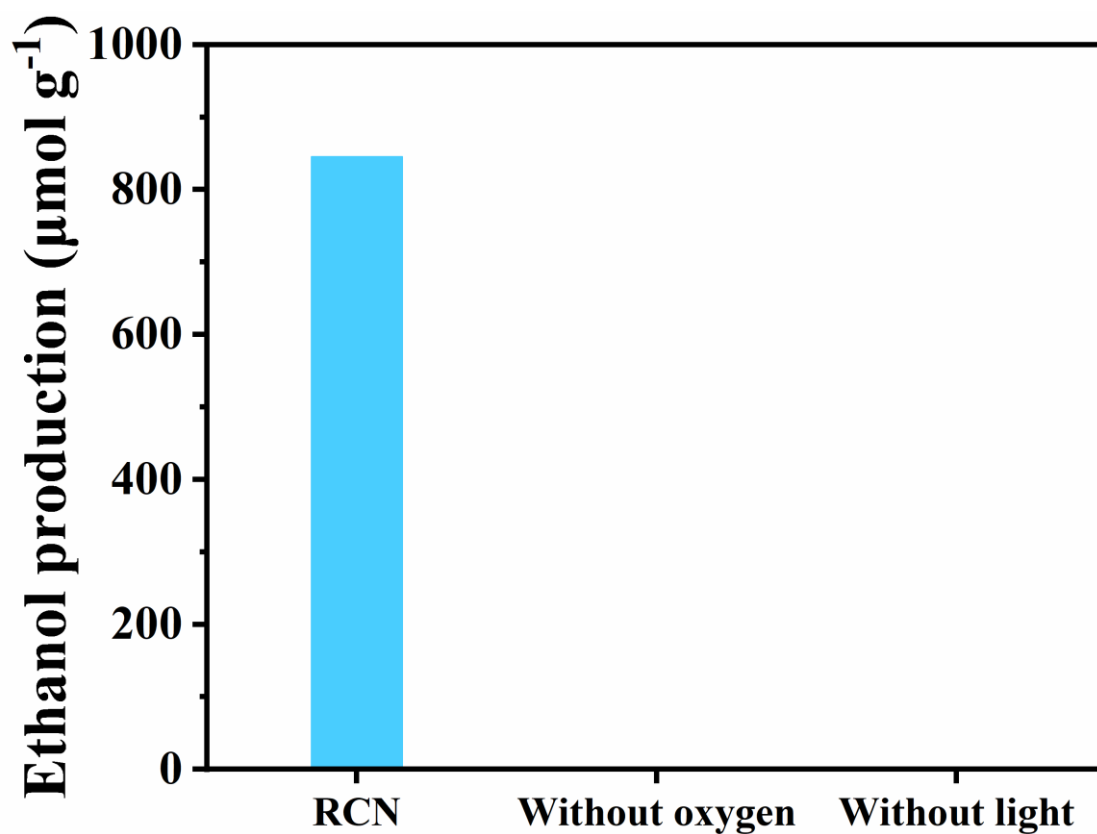


Figure S10. Control experimental results of the photocatalytic reaction over RCN-5.

The control experiments were carried out to illustrate the crucial role of oxygen and light. Without oxygen or light, no obvious ethanol production could be observed. The results revealed that both oxygen and light played a significant role in efficient photocatalytic methane conversion.

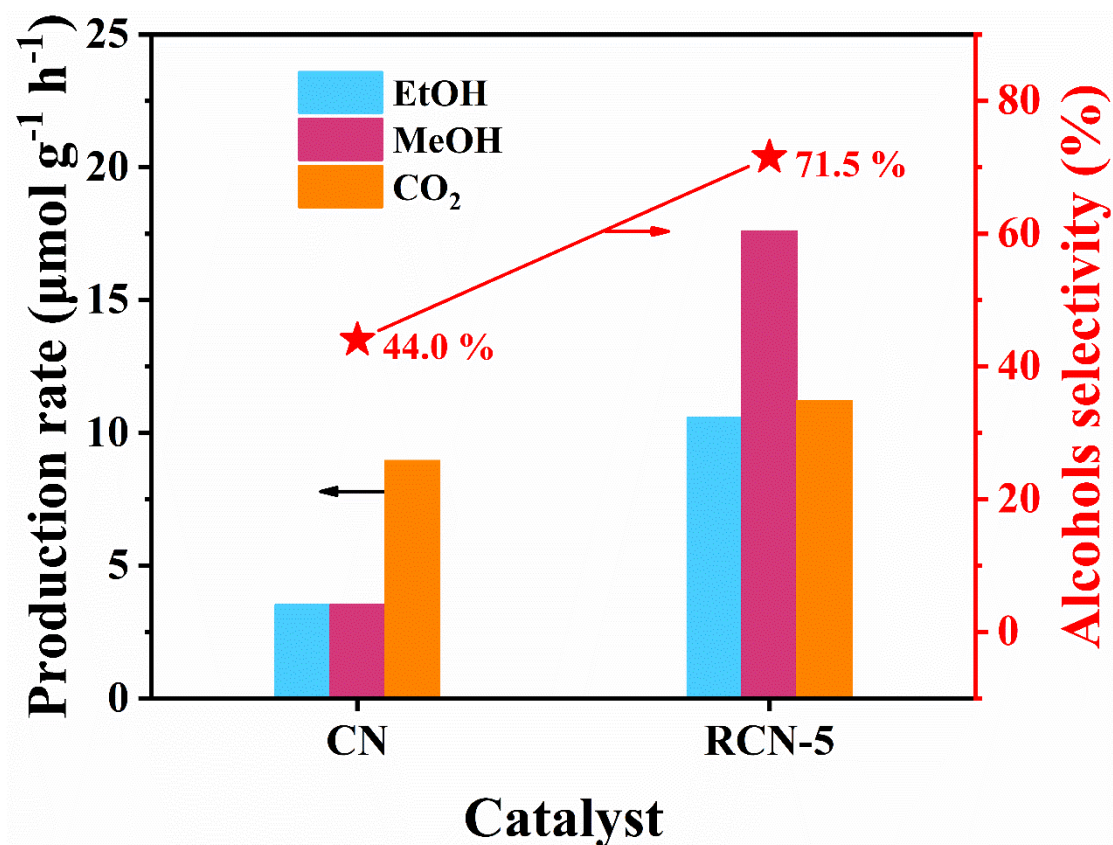


Figure S11. Average production rate of methane conversion over CN and RCN-5 samples in 10 h without illumination.

Reaction conditions: 20 mg catalysts; 1 mM H₂O₂, 20 mL; 2.0 MPa CH₄; temperature, 25±1 °C; reaction time, 10 h.

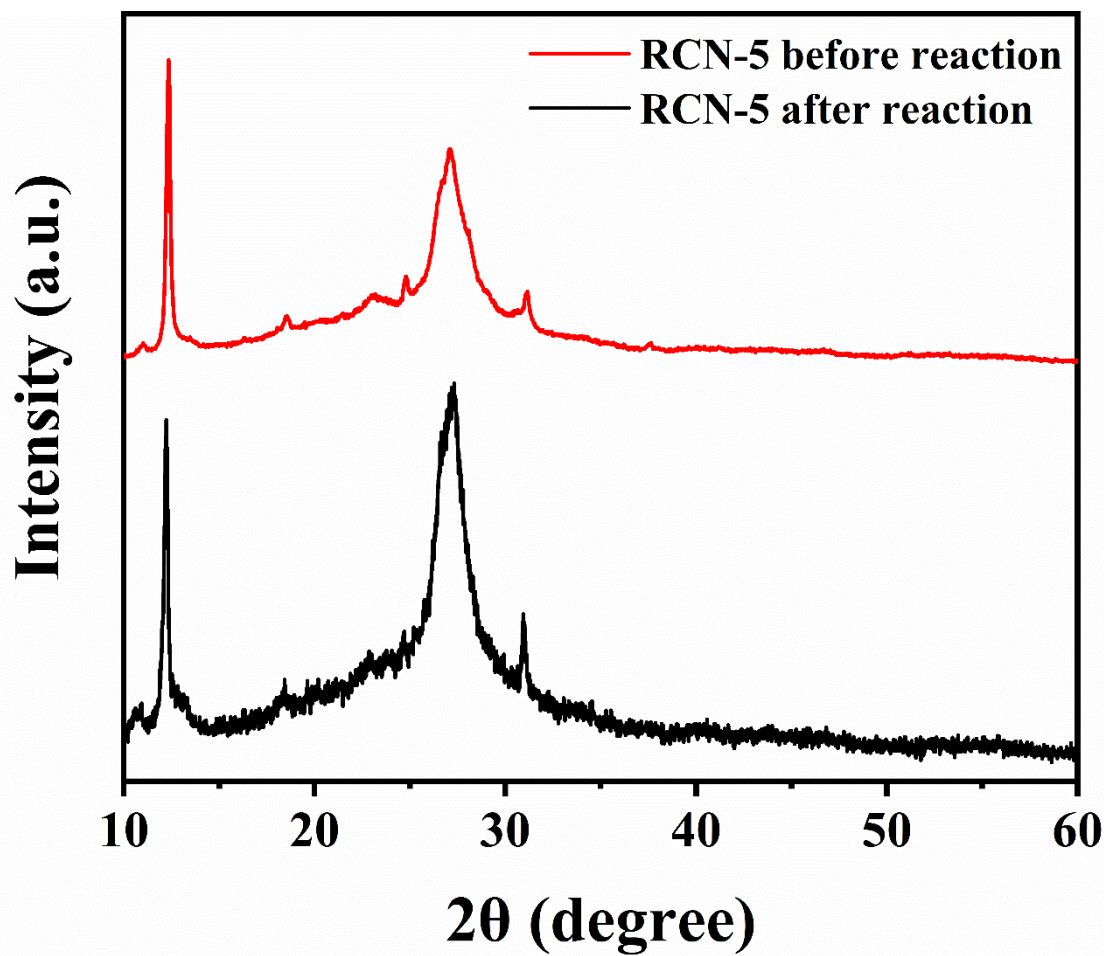


Figure S12. XRD patterns of RCN-5 before and after reaction.

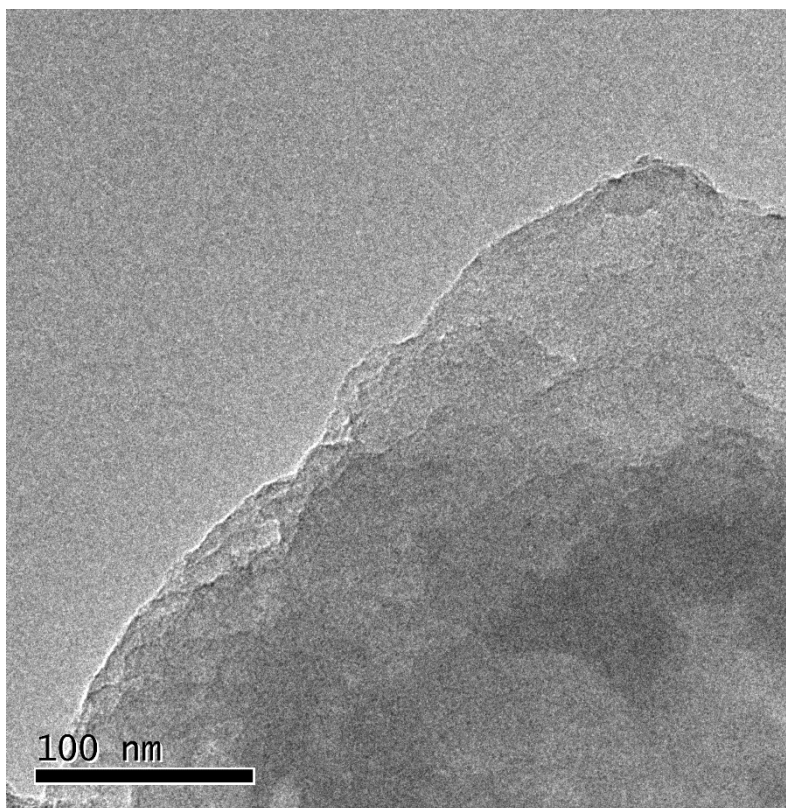


Figure S13. TEM image of RCN-5 after reaction.

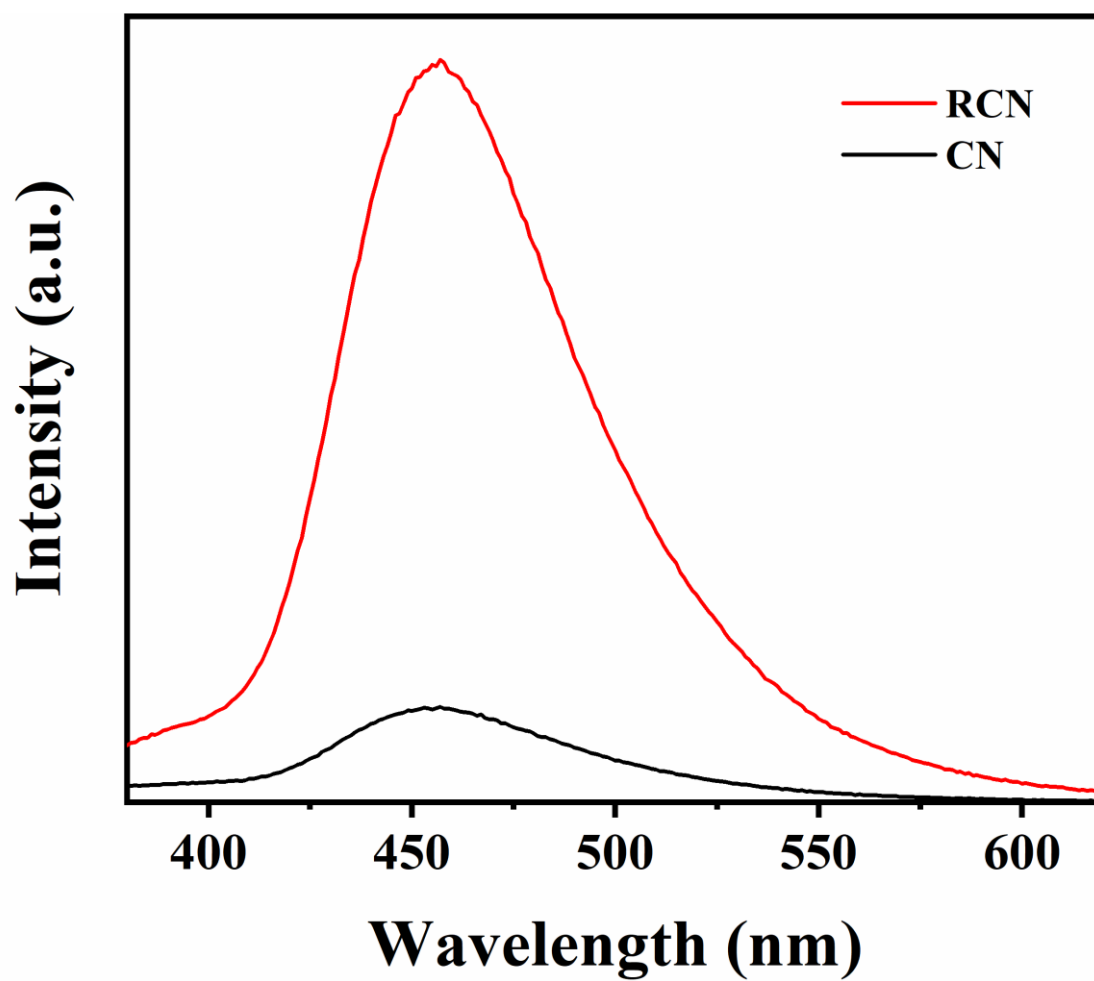


Figure S14. PL spectra of 1 mM coumarin solution over CN and RCN-5.

The fluorescence peaks are located at 456.6 nm under 332 nm excitation.^[3]

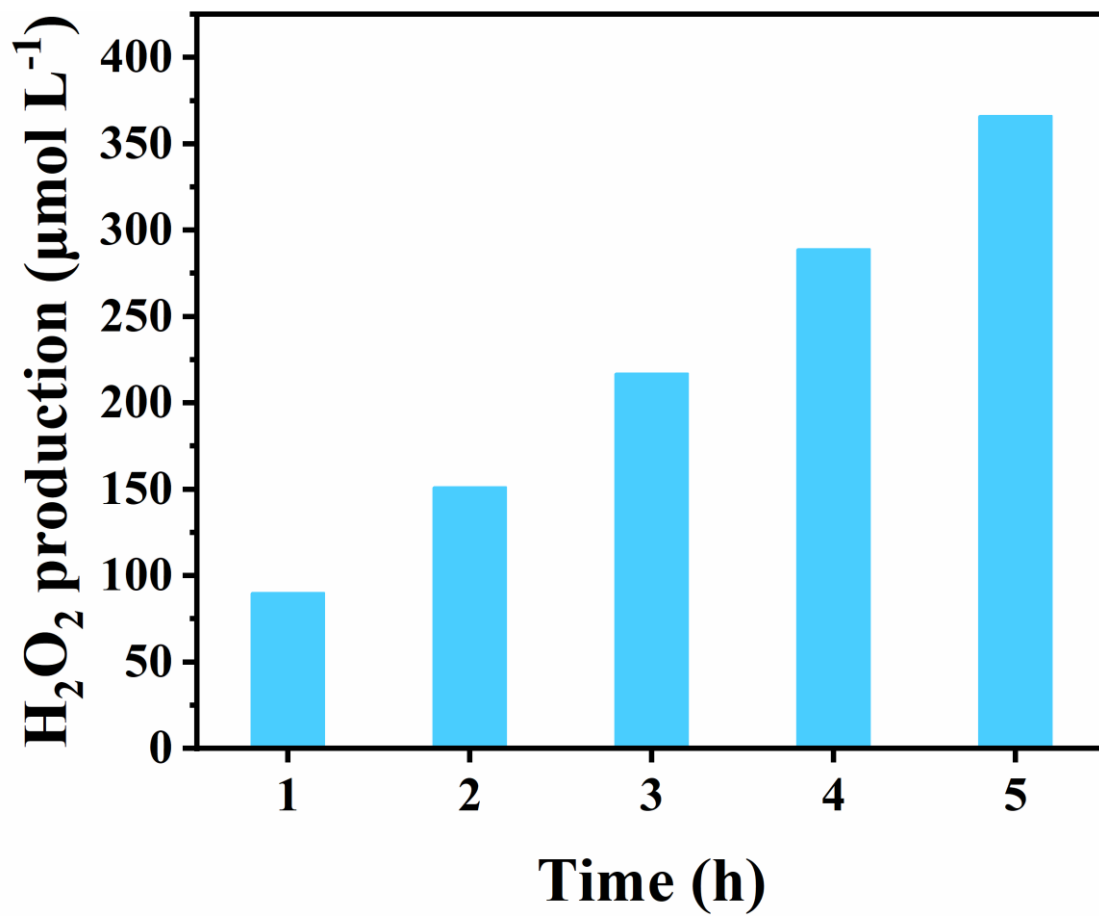


Figure S15. Photocatalytic H₂O₂ production over RCN-5 with different reaction time.

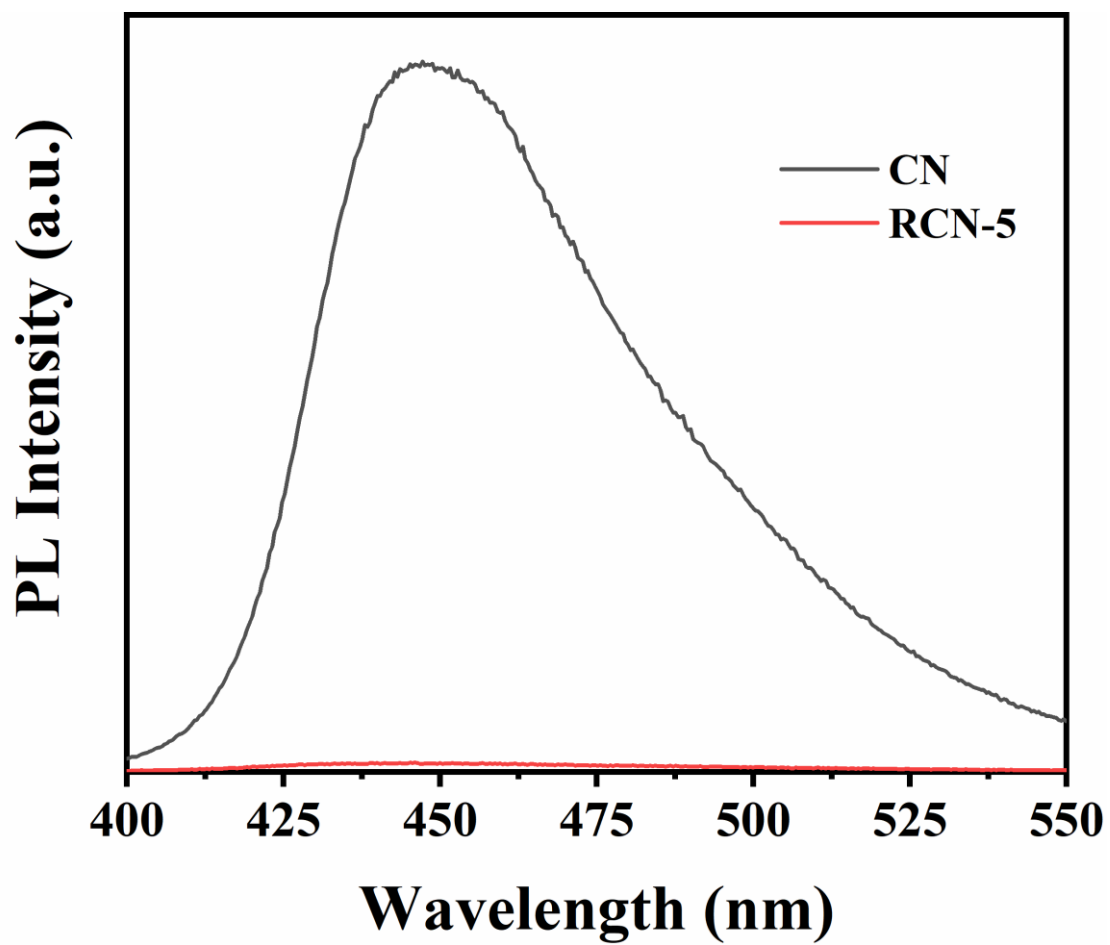


Figure S16. PL spectra of CN and RCN-5.

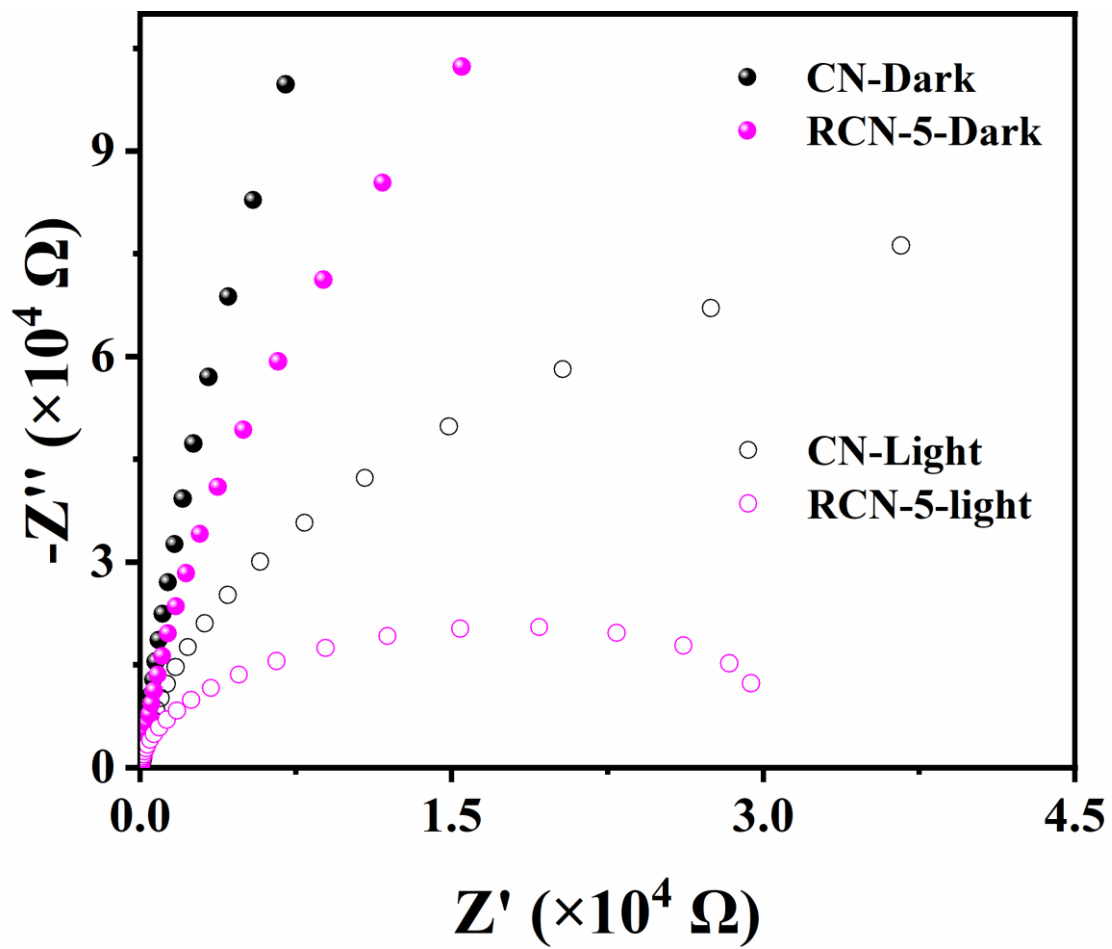


Figure S17. Electrochemical impedance spectroscopy for CN and RCN-5.

Table S1. Comparison of photocatalytic conversion of methane into ethanol over various catalyst reported at room temperature.

Catalysts	Reaction conditions			Ethanol production rate ($\mu\text{mol g}^{-1} \text{h}^{-1}$)	Ethanol selectivity (%)	Ref.
	Reactants	Temp. ($^{\circ}\text{C}$)	Light source			
commercial	25% CH ₄ , 75% N ₂ , 0.1 MPa	room	185 nm low-pressure	-	26.34	[4]
Beta zeolite	20 mg cat., 25 ml H ₂ O	temperature	mercury lamp			
Cu-0.5/PCN	CH ₄ /N ₂ , 10/90 ml min ⁻¹ , 0.1 MPa	room	visible light	106	81.2	[5]
	20 mg cat., 25 ml H ₂ O	temperature				
CeO ₂ -1100	4 ml min ⁻¹ CH ₄ , 0.02 MPa	25	300 W Xe lamp	11.4	91.5	[6]
	2 mg cat., 15 ml H ₂ O		light intensity: 100 mW cm ⁻²			
RCN-5	0.1 MPa O ₂ , 2 MPa CH ₄	25±1	300 < λ < 800 nm	281.6	85.1	this work
	20 mg cat., 20 ml H ₂ O		light intensity: 100 mW cm ⁻²			

Table S2. C/N atomic ratio of CN and RCN samples from EA results.

Samples	C (wt%)	N (wt%)	C/N atomic ratio
CN	28.86	53.64	0.63
RCN-3	29.47	52.12	0.66
RCN-5	28.23	46.36	0.71
RCN-7	29.14	45.58	0.75

Table S3. C/N atomic ratio of CN and RCN samples from XPS analysis.

Samples	C (Atom conc%)	N (Atom conc%)	C/N atomic ratio
CN	38.86	61.14	0.64
RCN-3	40.45	59.55	0.68
RCN-5	41.40	58.60	0.71
RCN-7	42.56	57.44	0.74

Table S4. The multi-exponential fitting results of fluorescence decay for CN and RCN-5.

Samples	A1	τ_1 (ns)	A2	τ_2 (ns)	A3	τ_3 (ns)	τ (ns)
CN	0.18	28.018 ± 0.428	0.01	56.036 ± 2.732	0.81	5.138 ± 0.036	10.18
RCN-5	0.16	10.847 ± 0.168	0.01	134.262 ± 2.068	0.84	2.086 ± 0.021	4.38

Reference

- [1] Z. Zhu, H. Pan, M. Murugananthan, J. Gong, Y. Zhang, *Appl. Catal., B*, 2018, 232, 19-25.
- [2] G. Liu, T. Wang, S. Ouyang, L. Liu, H. Jiang, Q. Yu, T. Kako, J. Ye, *J. Mater. Chem. A*, **2015**, 3, 8123-8132.
- [3] Q. Xiang, J. Yu, P. K. Wong, *J. Colloid Interface Sci.*, **2011**, 357, 163-167.
- [4] F. Sastre, V. Fornes, A. Corma, H. Garcia, *Chem. Eur. J.*, **2012**, 18, 1820-1825.
- [5] Y. Zhou, L. Zhang, W. Wang, *Nat. Commun.*, **2019**, 10, 506.
- [6] J. Du, W. Chen, G. Wu, Y. Song, X. Dong, G. Li, J. Fang, W. Wei, Y. Sun, *Catalysts* **2020**, 10, 196.